

# Numerical study of large-scale vorticity generation in shear-flow turbulence

Petri J. Käpylä\*

*Observatory, Tähtitorninmäki (PO Box 14), FI-00014 University of Helsinki, Helsinki, Finland*

Dhrubaditya Mitra†

*Astronomy unit, School of Mathematical Sciences, Queen Mary, University of London, Mile End Road, London E1 4NS, United Kingdom*

Axel Brandenburg‡

*NORDITA, Roslagstullsbacken 23, SE-10691 Stockholm, Sweden*

(Received 7 October 2008; published 9 January 2009)

Simulations of stochastically forced shear-flow turbulence in a shearing-periodic domain are used to study the spontaneous generation of large-scale flow patterns in the direction perpendicular to the plane of the shear. Based on an analysis of the resulting large-scale velocity correlations it is argued that the mechanism behind this phenomenon could be the mean-vorticity dynamo effect pioneered by Elperin, Kleeorin, and Rogachevskii [Phys. Rev. E **68**, 016311 (2003)]. This effect is based on the anisotropy of the eddy viscosity tensor. One of its components may be able to replenish cross-stream mean flows by acting upon the streamwise component of the mean flow. Shear, in turn, closes the loop by acting upon the cross-stream mean flow to produce stronger streamwise mean flows. The diagonal component of the eddy viscosity is found to be of the order of the rms turbulent velocity divided by the wave number of the energy-carrying eddies.

DOI: [10.1103/PhysRevE.79.016302](https://doi.org/10.1103/PhysRevE.79.016302)

PACS number(s): 47.27.tb, 47.27.ek, 95.30.Lz

## I. INTRODUCTION

The imperfect analogy between the induction equation and the vorticity equation has always raised questions regarding the extent of this analogy. While it is well-known that the averaged induction equation for the mean magnetic field admits self-excited solutions for a turbulent flow with helicity, analogous solutions to the averaged vorticity equation only exist in the compressible case [1,2]. An exception is the case of flows that are driven by a non-Galilean invariant forcing function, which can give rise to the so-called anisotropic kinetic  $\alpha$  effect [3–6]. This effect produces mean flows that are helical and of Beltrami type. Another example of mean flow generation is the  $\Lambda$  effect [7,8], whereby large-scale nonuniform flows can be produced in rotating anisotropic turbulence.

In the last few years another example has emerged, where the analogy between vorticity and induction equations is more striking. This example applies to the case of shear-flow turbulence. In fact, it has been argued that large-scale magnetic field generation is possible via the shear-current effect that results from nonvanishing off-diagonal components of the turbulent magnetic diffusivity tensor [9,10]. This effect predicts large-scale field generation in homogeneous shear-flow turbulence with nonhelical driving, which has indeed been seen in several simulations [11–13]. However, there is the problem that, according to the test-field method, the sign of the relevant component of the turbulent magnetic diffusivity tensor was found to be incompatible with that required

for the shear-current dynamo [12]. On the other hand, the analogous hydrodynamic effect has not yet been explored in sufficient detail. This effect may explain the generation of large-scale vorticity in homogeneous shear-flow turbulence and was first studied analytically in a seminal paper by Elperin, Kleeorin, and Rogachevskii [14]. Several recent studies discuss numerical evidence for the spontaneous formation of mean vorticity [11–13]. In those papers the main objective is to study the generation of large-scale magnetic fields by shear-flow turbulence, while the simultaneous generation of mean vorticity was merely an additional (but interesting) complication. On the other hand, in view of the disappointing experience when trying to verify the operation of the shear-current dynamo using the test-field method, one should be careful in view of earlier negative results [15] concerning both the shear-current effect and the mean-vorticity dynamo effect. The aim of this paper is therefore to discuss turbulent shear flow simulations without magnetic fields in order to demonstrate the existence of the mean-vorticity dynamo and to analyze its connection with the eddy viscosity tensor in more detail.

Following earlier work [11–13], periodic boundary conditions are used in the streamwise direction and in the direction perpendicular to the plane of the shear, while shearing-periodic boundary conditions are used in the cross-stream direction. This means that mass and mean momentum are conserved. Furthermore, if a large-scale flow emerges, it will also be periodic corresponding to a simple sine wave. The mean vorticity is therefore also a long-wavelength sine wave. However, although the original analysis was based on mean vorticity, we discuss in the following mainly the mean velocity, because the corresponding equations are simpler and more intuitive.

For a proper analysis of the hydrodynamic mean-vorticity dynamo effect one would need to proceed analogously to the

\*petri.kapyla@helsinki.fi

†dhruba.mitra@gmail.com

‡brandenb@nordita.org

hydromagnetic case where it was possible to determine all relevant components of the turbulent magnetic diffusivity tensor using the test-field method. One would then need to determine all relevant components of the eddy viscosity tensor. However, in the absence of a properly developed “test-flow” method for hydrodynamics, we must resort to more primitive measures for estimating components of the eddy viscosity tensor. Using decay calculations of a large-scale velocity structure, it was found that eddy viscosity  $\nu_t$  and turbulent magnetic diffusivity  $\eta_t$  are approximately equal, i.e.,  $\nu_t \approx \eta_t$ , and around  $(0.8-0.9) \times u_{\text{rms}}/k_f$  [16]. Here,  $k_f$  is the wave number corresponding to the scale of the energy-carrying eddies and  $u_{\text{rms}}$  is the rms velocity of the turbulence. On the other hand, a more accurate determination of  $\eta_t$  led recently to the  $\eta_t = \eta_{t0} \equiv u_{\text{rms}}/(3k_f)$ , where  $\eta_{t0}$  is just a reference value. In this paper we use an analogously defined reference value,  $\nu_{t0} \equiv u_{\text{rms}}/(3k_f)$ , but note that there is no strong case for assuming that  $\nu_t$  will be close to  $\nu_{t0}$ .

## II. THE MODEL

In the present work we consider weakly compressible subsonic turbulence in the presence of a linear shear flow

$$\bar{\mathbf{U}}^S = (0, Sx, 0), \quad (1)$$

so  $x$  is the cross-stream direction,  $y$  is the streamwise direction, and  $z$  is the direction perpendicular to the plane of the shear flow. Since the effect of temperature changes is not important in this context, we consider an isothermal equation of state. In the following we work with the departures from this mean flow, so the total velocity is  $\bar{\mathbf{U}}^S + \mathbf{U}$ , and the governing equations for  $\mathbf{U}$  are then [12]

$$\frac{D\mathbf{U}}{Dt} = -S\mathbf{U}_x \hat{\mathbf{y}} - c_s^2 \nabla \ln \rho + \mathbf{f} + \mathbf{F}_{\text{visc}}, \quad (2)$$

$$\frac{D \ln \rho}{Dt} = -\nabla \cdot \mathbf{U}, \quad (3)$$

where  $D/Dt = \partial/\partial t + (\bar{\mathbf{U}}^S + \mathbf{U}) \cdot \nabla$  is the advective derivative with respect to the total velocity,  $c_s$  is the isothermal sound speed, here considered as constant,  $\rho$  is the mass density,  $\mathbf{f}$  is a random forcing function,  $\mathbf{F}_{\text{visc}} = \rho^{-1} \nabla \cdot 2\rho\nu\mathbf{S}$  is the viscous force, and  $\mathbf{S}_{ij} = \frac{1}{2}(U_{i,j} + U_{j,i}) - \frac{1}{3}\delta_{ij} \nabla \cdot \mathbf{U}$  is the traceless rate of strain tensor and commas denote partial derivatives.

The forcing function is  $\delta$  correlated in time and consists of random plane waves with wave vectors  $\mathbf{k}$  in the interval  $4.5 \leq k/k_1 \leq 5.5$  [17]. During each time step,  $\mathbf{f}$  is a single transverse (solenoidal) plane wave proportional to  $\mathbf{k} \times \mathbf{e}$ , where the wave vector  $\mathbf{k}$  is taken randomly from a set of predefined vectors with components that are integer multiples of  $2\pi/L$  and whose moduli are in a certain interval around an average value  $\langle |\mathbf{k}| \rangle$ , which we denote by  $k_f$ , and  $\mathbf{e}$  is an arbitrary random unit vector not aligned with  $\mathbf{k}$ . The corresponding scale  $2\pi/k_f$  is referred to as the energy-carrying scale of the turbulence. Moreover, the time dependence of  $\mathbf{f}$  is designed to mimic  $\delta$ -correlation, which is a simple and commonly used form of random driving [17].

There are two important dimensionless control parameters, the Reynolds number  $\text{Re}$  and the shear parameter  $\text{Sh}$ ,

$$\text{Re} = u_{\text{rms}}/(\nu k_f), \quad \text{Sh} = S/(u_{\text{rms}} k_f), \quad (4)$$

that quantify the intensity of turbulence and shear, respectively. We note that the values of  $\text{Re}$  and  $\text{Sh}$  cannot be chosen a priori due to the strong effect that the vorticity dynamo has on the value of  $u_{\text{rms}}$  in the saturated state. Thus we always refer to values of  $u_{\text{rms}}$ ,  $\text{Re}$ , and  $\text{Sh}$  that apply to the situation where the vorticity dynamo is absent, i.e., early stages of the run or a nonshearing simulation. The ratio of the size of the domain  $L$  to the size of the energy-carrying scale is also an important control parameter that we call the scale separation ratio, written here as  $k_f L / 2\pi = k_f / k_1$ , where  $k_1 = 2\pi/L$  is the smallest wave number that fits into the domain.

We employ the PENCIL code [18] with sixth-order finite differences in space and a third order time stepping scheme. We use triply-periodic boundary conditions, except that the  $x$  direction is shearing periodic, i.e.,

$$\mathbf{U}\left(-\frac{1}{2}L_x, y, z, t\right) = \mathbf{U}\left(\frac{1}{2}L_x, y + L_x S t, z, t\right). \quad (5)$$

This condition is routinely used in numerical studies of shear flows in Cartesian geometry [19,20].

## III. RESULTS

The initial velocity is zero, but the volume forcing drives a random flow that soon develops a turbulent cascade where the spectral energy follows an approximate  $k^{-5/3}$  inertial range between the forcing wave number  $k_f$  and some dissipation wave number  $k_d = (\mathbf{S}^2/\nu^2)^{1/4}$ .

In Fig. 1 we show images of the streamwise component of  $\mathbf{U}$  at the periphery of the computational domain from a run with  $\text{Re} \approx 100$  and  $\text{Sh} \approx -0.2$  (hereafter Run A). At early times the velocity pattern is dominated by structures whose scale is comparable with the forcing scale, which is about one fifth of the domain size. However, at later times there is a tendency to produce large-scale flow patterns with a long wavelength variation in the  $z$  direction. This flow pattern tends to be unstable and keeps disappearing and reappearing. This is seen also for other runs with smaller Reynolds number.

Given the systematic variation in the  $z$  direction, it is useful to consider averages over the  $x$  and  $y$  directions, denoted in the following by overbars. So,  $\bar{\mathbf{U}} = \bar{\mathbf{U}}(z, t)$  depends only on  $z$  and  $t$ . Figure 2 shows  $\bar{U}_x$  and  $\bar{U}_y$  as functions of time and  $z$ . In Fig. 3 we plot the  $z$  dependence of  $\bar{U}_x$  and  $\bar{U}_y$  at a time near the maximum vorticity. Note that the amplitude of  $\bar{U}_y$  is about 4 times as big as that of  $\bar{U}_x$ , and that the two fields are essentially in phase. The fact that  $\bar{U}_x$  and  $\bar{U}_y$  are in phase is an immediate consequence of the fact that  $S < 0$ , and that there is a minus sign in front of  $S$  in Eq. (2).

In run A with  $512^3$  meshpoints there is one particularly pronounced event during the time interval  $200 < tu_{\text{rms}}k_f < 400$ , where  $\bar{U}'_y$  reaches an extremum at  $tu_{\text{rms}}k_f \approx 280$ , followed by an extremum of  $\bar{U}'_x$  a bit later at  $tu_{\text{rms}}k_f \approx 300$ ; see

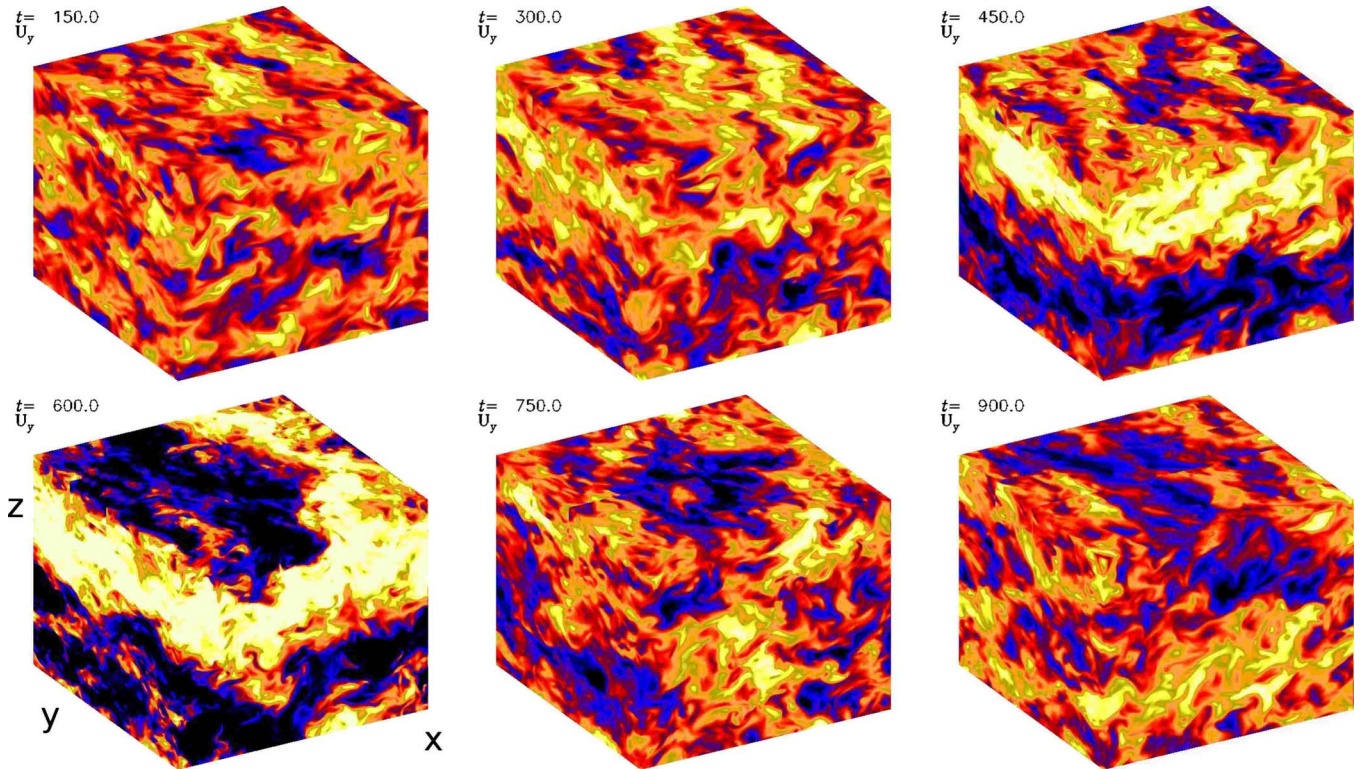


FIG. 1. (Color online) Representation of  $U_y$  on the periphery of the computational domain for run A at six different times showing the occasional generation of large scale flow patterns with a systematic variation in the  $z$  direction. Dark (blue) shades refer to negative values of  $U_y$  while light (yellow) shades refer to positive values. Note that at time  $tc_s k_1 = 900$  (corresponding to  $tu_{rms} k_f \approx 480$ ) the orientation of the flow pattern in the  $z$  direction is reversed compared to the previous event at  $tc_s k_1 = 600$  (corresponding to  $tu_{rms} k_f \approx 300$ ).

Fig. 4 for their root mean square values. Here, derivatives with respect to  $z$  are denoted by a prime.

The occasional extrema in the components of  $\bar{U}$  and its derivatives are accompanied by strong enhancements in the rms value of the total velocity  $U_{rms}$ , which includes the mean flow as well. This fact has been of some significance in previous studies of hydromagnetic dynamo action from turbulent shear flows [11,13,21], because, depending on the value of the sound speed, this can lead to numerical difficulties if the Mach number exceeds unity during these strong enhancements of  $U_{rms}$ . These difficulties are here avoided by choos-

ing a smaller shear parameter  $Sh$ , regulated by the input parameter  $S$ .

The effect of increasing  $S$  is demonstrated in Fig. 5, which shows the rms values of the large-scale velocities for four runs where  $S$  is varied while the other parameters are kept constant. The amount of shear is here quantified by the value of  $Sh$ , which is based on the  $u_{rms}$  value from a run without shear and thus effectively quantifies the strength of the random forcing. These runs are denoted by the letters B–E, with the strength of the shear increasing from  $Sh = -0.08$  in run B

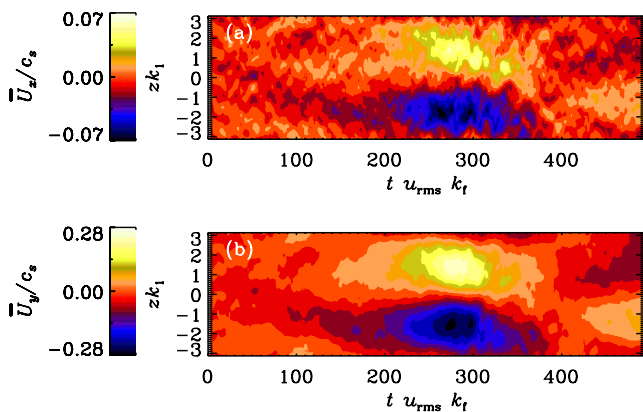


FIG. 2. (Color online)  $\bar{U}_x$  (a) and  $\bar{U}_y$  (b) as functions of time and  $z$  for run A.

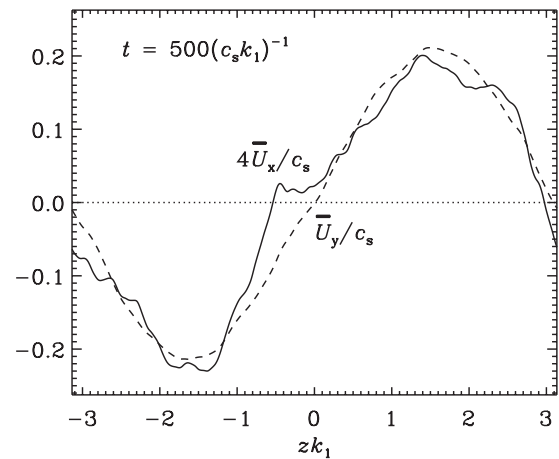


FIG. 3. Four times  $\bar{U}_x$  (solid line) and  $\bar{U}_y$  (dashed) from run A at  $t = 500(c_s k_1)^{-1}$ .

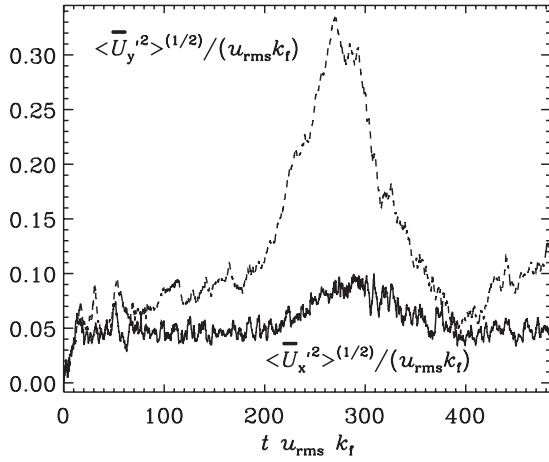


FIG. 4. Root mean square values of  $\bar{U}'_x$  (solid line) and  $\bar{U}'_y$  (dashed line) for run A. Note the maxima at  $tu_{\text{rms}}k_f \approx 280$  and  $tu_{\text{rms}}k_f \approx 260$ , respectively.

to  $\text{Sh} = -0.33$  in run E. The bottom panel of Fig. 5 shows that  $U_{\text{rms}}$  increases almost in proportion to the shear for  $-\text{Sh} > 0.25$ . The flow in the large  $\text{Sh}$  runs is also highly fluctuating during periods of vigorous vorticity generation, see Fig. 6 for a space-time diagram of the large-scale velocities from run E. Even in the lowest shear run (run B with  $\text{Sh} \approx -0.08$ ), which is very similar to the nonshearing case during most of its evolution, a weak large-scale pattern is discernible at times, see times after  $tu_{\text{rms}}k_f > 600$  in Fig. 7.

#### IV. INTERPRETATION

In order to shed some light on the mechanism responsible for the generation of large-scale vorticity, we consider mean-field equations [14,22]. Adopting averages over the  $(x, y)$  plane, denoted here by an overbar, we have

$$\frac{\partial \bar{U}}{\partial t} = -S \bar{U}_y \hat{y} + \bar{\mathcal{F}} + \nu \bar{U}''', \quad (6)$$

where  $\bar{\mathcal{F}} = -\overline{\mathbf{u} \cdot \nabla \mathbf{u}}$  is a term that results from the nonlinearity of the Navier-Stokes equations, and primes denote a  $z$  derivative. Note that we have assumed solenoidality, i.e.,  $\nabla \cdot \bar{U} = \bar{U}_{3,3} = 0$ , so  $\bar{U}_3 = \text{const.} = 0$  by a suitable choice of the initial condition. Thus, only the  $x$  and  $y$  components of  $\bar{U}$  are nonvanishing. Therefore,  $\bar{U} \cdot \nabla \bar{U} = 0$ . Furthermore, the pressure gradient term does not enter in Eq. (6), because any horizontally averaged gradient term can only have a  $z$  component. Using mean field theory [14],  $\bar{\mathcal{F}}$  can be expressed in terms of derivatives of the mean flow. In the present case of one-dimensional mean fields this relationship reduces to

$$\bar{\mathcal{F}}_i = \nu_{ij} \bar{U}_j'', \quad (7)$$

where  $\nu_{ij}$  is the eddy viscosity tensor. We also assume incompressibility of the small-scale velocity field  $\nabla \cdot \mathbf{u} = 0$ , which is a good approximation for small Mach numbers, and recall that horizontal averages depend only on  $z$ , i.e., the  $j = 3$  coordinate. Therefore we have

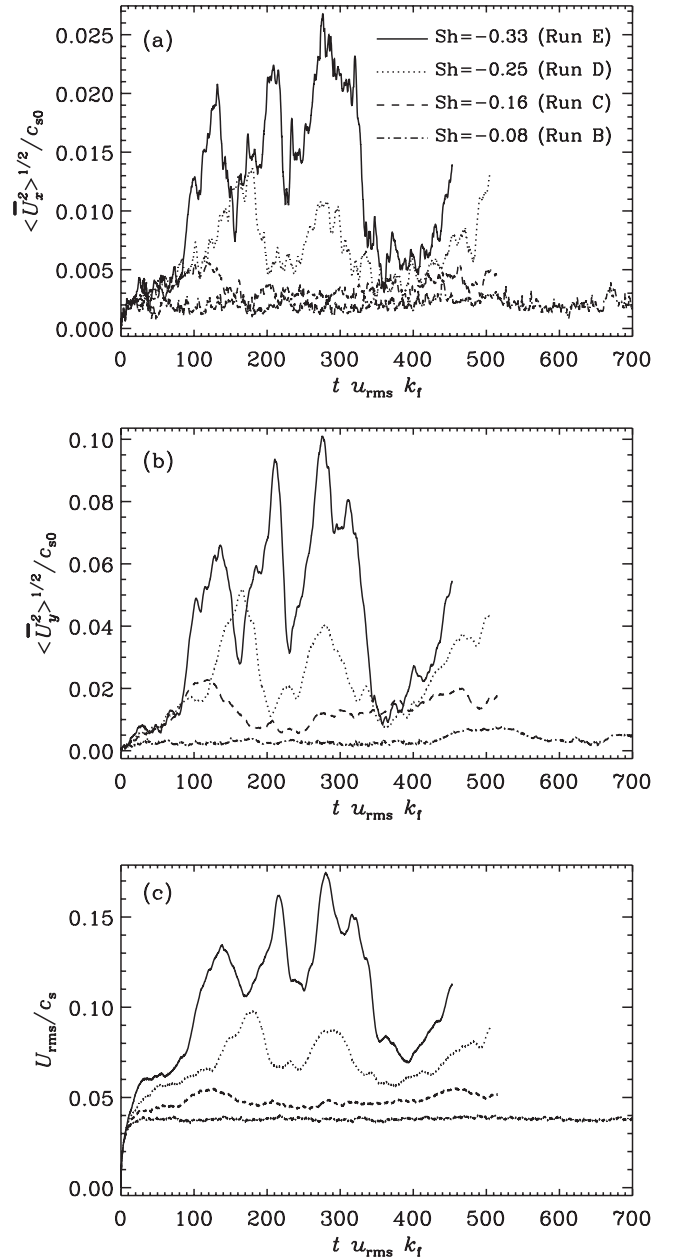


FIG. 5. Root mean square values of  $\bar{U}'_x$  (a) and  $\bar{U}'_y$  (b), and  $U_{\text{rms}}$  (c) for runs B-E with different shear as indicated in the legend in panel (a). The Reynolds number based on the  $u_{\text{rms}}$  from a nonshearing run is  $\approx 24$ .

$$\bar{\mathcal{F}}_i = -\nabla_3 \overline{u_i u_3} = -\bar{\mathcal{R}}_i'. \quad (8)$$

Here we have denoted the two relevant components of the Reynolds stress tensor by  $\bar{\mathcal{R}}_i \equiv \overline{u_i u_3}$ , where  $i = 1, 2$  refer to the  $x$  and  $y$  directions and  $u_3$  is the  $z$  component of the velocity fluctuation. Integrating Eq. (7) over  $z$ , we have

$$\bar{\mathcal{R}}_i + \nu_{ij} \bar{U}_j' \equiv \text{const.} \quad (9)$$

Given that  $\bar{\mathcal{R}}$  and  $\bar{U}$  can be obtained from the simulations, we can then find all four components of  $\nu_{ij}$  by considering moment equations of the form

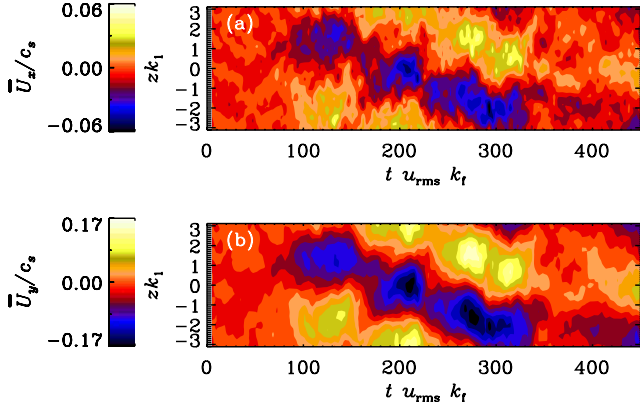


FIG. 6. (Color online)  $\bar{U}_x$  (a) and  $\bar{U}_y$  (b) as functions of time and  $z$  for run E with  $\text{Sh} \approx -0.33$ .

$$\langle \bar{\mathcal{R}}_i \bar{U}'_k \rangle + \nu_{ij} \mathbf{M}_{jk} = 0, \quad (10)$$

where we have introduced the correlation matrix  $\mathbf{M}_{jk} = \langle \bar{U}'_j \bar{U}'_k \rangle$ . We have also assumed that  $\nu_{ij}$  is independent of  $z$ , and that, owing to periodic boundary conditions, the mean flow and its  $z$  derivatives have zero volume average, i.e.,  $\langle \bar{U}'_i \rangle = 0$  for any  $i$ . The components of  $\nu_{ij}$  can then be written as

$$\begin{pmatrix} \nu_{i1} \\ \nu_{i2} \end{pmatrix} = -\mathbf{M}^{-1} \begin{pmatrix} \langle \bar{\mathcal{R}}_1 \bar{U}'_i \rangle \\ \langle \bar{\mathcal{R}}_2 \bar{U}'_i \rangle \end{pmatrix}, \quad (11)$$

where  $i=1$  or  $2$ .

It turns out that the components of the correlations  $\langle \bar{\mathcal{R}}_1 \bar{U}'_j \rangle$  are small compared with those of  $\mathbf{M}_{jk}$ . This makes the evaluation of the components of  $\nu_{ij}$  using Eq. (11) ill behaved (see Fig. 8). This procedure does, however, yield reasonable results for the  $\nu_{2i}$  components:  $\nu_{21}$  is highly fluctuating, but with an average of the order of roughly half of the reference value  $\nu_{i0} \equiv \frac{1}{3} u_{\text{rms}} k_f^{-1}$ , whereas  $\nu_{22}$  is positive and between one and two times  $\nu_{i0}$  in the quiescent phases of the simulation and peaking at roughly  $5\nu_{i0}$  when the vorticity peaks. The definition of  $\nu_{i0}$  is analogous to a corresponding

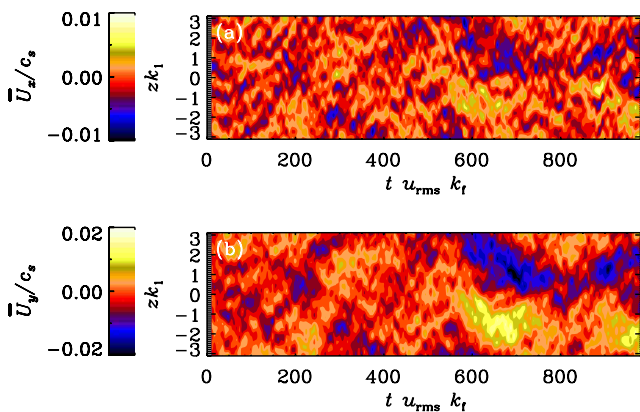


FIG. 7. (Color online)  $\bar{U}_x$  (a) and  $\bar{U}_y$  (b) as functions of time and  $z$  for run B with  $\text{Sh} \approx -0.08$ .

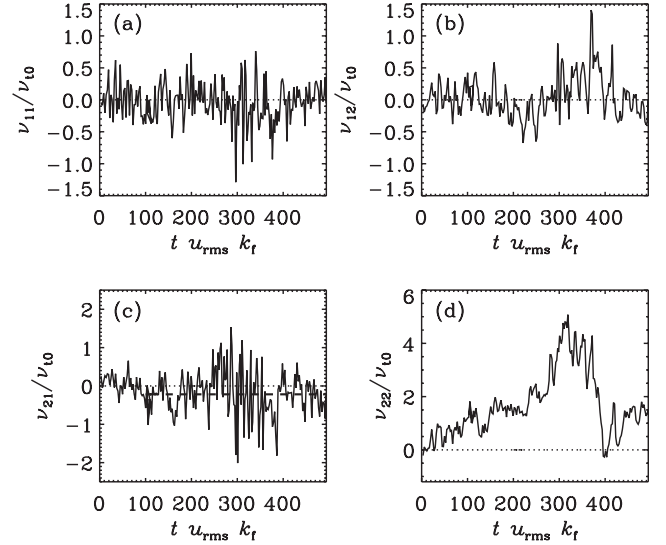


FIG. 8. Components of the eddy viscosity tensor as obtained from Eq. (11) normalized by  $\nu_{i0} = \frac{1}{3} u_{\text{rms}} k_f^{-1}$  for run A. Note that the average value of  $\nu_{21}$  is negative (see the dashed line in the third panel for  $t u_{\text{rms}} k_f > 100$ ).

reference value for the magnetic diffusivity [23], but it is not clear that  $\nu_i$  should be exactly equal to  $\nu_{i0}$  in any limit. Instead, according to the first order smoothing approximation,  $\nu_i = 0.4\nu_{i0}$  [16], and hence the magnetic Prandtl number was expected to be 0.4.

If both components of  $\langle \bar{\mathcal{R}}_1 \bar{U}'_k \rangle$  for  $k=1$  and  $2$  were exactly zero, we could calculate  $\nu_{12}/\nu_{11}$  in terms of the ratios

$$\frac{\nu_{12}}{\nu_{11}} = -\frac{\mathbf{M}_{1k}}{\mathbf{M}_{2k}} \quad (12)$$

for  $k=1$  and  $2$ . Yet another possibility is to take the geometric mean of the two expressions, so

$$\frac{\nu_{12}}{\nu_{11}} \approx -\left(\frac{\mathbf{M}_{11} \mathbf{M}_{12}}{\mathbf{M}_{21} \mathbf{M}_{22}}\right)^{1/2} \equiv -\left(\frac{\mathbf{M}_{11}}{\mathbf{M}_{22}}\right)^{1/2}, \quad (13)$$

where we have used the fact that  $\mathbf{M}_{21} = \mathbf{M}_{12}$ . The results shown in Fig. 9 indicate that the two ratios in Eq. (12) give consistently negative values, although their moduli are different. Assuming that  $\nu_{11}$  is positive, which is reasonable, this result suggests that a negative  $\nu_{12}$  is present in the system with a modulus that is between 0.2 and 0.4 times the  $\nu_{11}$  component.

Finally, a completely different approach for obtaining estimates between the components of  $\nu_{ij}$  is to use the resulting mean-field equations, Eq. (6), and apply them to a hypothetical steady state. These equations are linear, which is a consequence of assuming the components of  $\nu_{ij}$  to be constant. In that case we can Fourier transform and obtain the two equations

$$(\nu + \nu_{11})k^2 \hat{U}_1 + \nu_{12}k^2 \hat{U}_2 = 0, \quad (14)$$

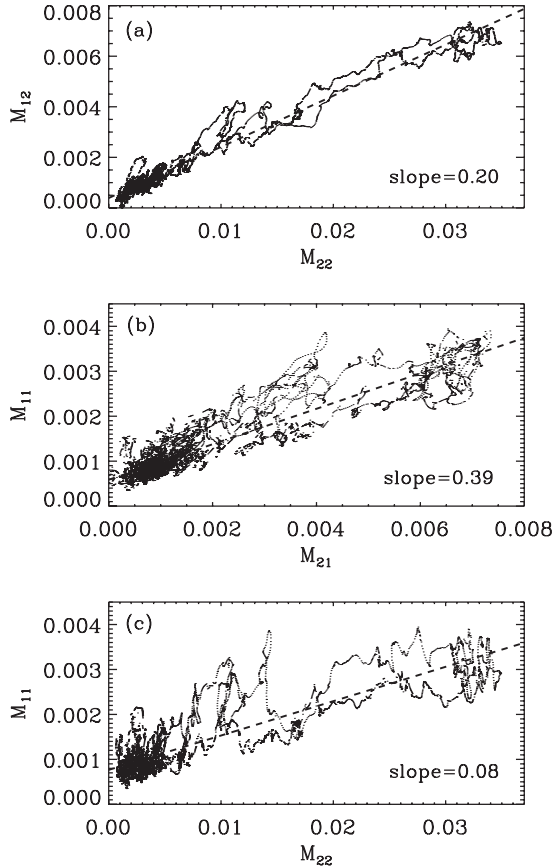


FIG. 9. Scatter plots of  $M_{12}/M_{22}$  (a),  $M_{11}/M_{21}$  (b),  $M_{11}/M_{22}$  (c) for run A.

$$(S + \nu_{21}k^2)\hat{U}_1 + (\nu + \nu_{22})k^2\hat{U}_2 = 0, \quad (15)$$

where  $\hat{U}_1$  and  $\hat{U}_2$  are the Fourier amplitudes of the  $x$  and  $y$  components of the mean flow. Since these equations are linear, they cannot describe nonlinear saturation of a mean-field vorticity dynamo instability. However, it is plausible that the assumption of constancy of the components  $\nu_{ij}$  breaks down when the resulting mean vorticity has become large enough. The resulting modifications of  $\nu_{ij}$  may then explain saturation.

Equations (14) and (15) show that a necessary condition for the mean-vorticity dynamo to be excited is that the product  $\nu_{12}S$  is positive. This is indeed the case; in our case both  $\nu_{12}$  and  $S$  are negative. A sufficient condition for the mean-vorticity dynamo to be excited is that the parameter

$$D \equiv [\nu_{12}(S/k^2 + \nu_{21}) + \epsilon^2]/\nu_T^2 \geq 1, \quad (16)$$

where  $\nu_T = \nu + \nu_t$  with

$$\nu_t = \frac{1}{2}(\nu_{11} + \nu_{22}), \quad \epsilon = \frac{1}{2}(\nu_{11} - \nu_{22}). \quad (17)$$

The parameter  $D$  plays the role of a mean-vorticity dynamo number. The assumption of a steady state in Eqs. (14) and (15) implies that  $D=1$ . Note that Eqs. (14) and (15) yield

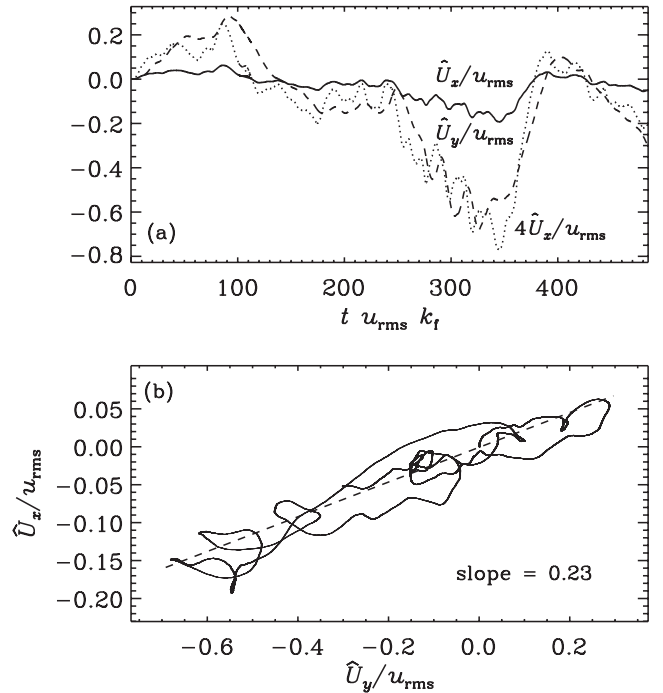


FIG. 10. (a):  $\hat{U}_x$  (solid line),  $4\hat{U}_x$  (dotted), and  $\hat{U}_y$  (dashed) as functions of time for run A. (b) scatter plot of  $\hat{U}_x$  versus  $\hat{U}_y$  for the same run. The dashed line shows a linear fit to the data.

$$\frac{\nu_{12}}{\nu + \nu_{11}} = -\frac{\hat{U}_1}{\hat{U}_2} = \frac{\nu + \nu_{22}}{S/k^2 + \nu_{21}}. \quad (18)$$

This allows us to calculate  $\nu + \nu_{22}$  in terms of  $u_{\text{rms}}/k_f$ , provided  $\nu_{21}$  is negligible or known:

$$\frac{\nu + \nu_{22}}{u_{\text{rms}}/k_f} = -\frac{\hat{U}_1}{\hat{U}_2} \left[ \text{Sh}\left(\frac{k_f}{k_1}\right)^2 + \frac{\nu_{21}k_f}{u_{\text{rms}}} \right]. \quad (19)$$

The amplitudes  $\hat{U}_1$  and  $\hat{U}_2$  for run A are shown in Fig. 10. Putting in numbers,  $\hat{U}_1/\hat{U}_2=0.23$ ,  $k_f/k_1=5$ , we obtain

$$\frac{\nu + \nu_{22}}{u_{\text{rms}}/k_f} = 1.15 - 0.23 \frac{\nu_{21}k_f}{u_{\text{rms}}}, \quad (20)$$

so the uncertainty in  $\nu_{21}$  enters only weakly. Note, however, that  $\nu_{22}$  is more than three times larger than the original estimate of  $\nu_0$ .

## V. EDDY VISCOSITY FROM THE IMPOSED SHEAR

We have so far only looked at the components of the Reynolds stress tensor that enter the horizontally averaged equations. However, there is at least one other component that does not enter Eq. (6), but that can also be used to determine the eddy viscosity (see, e.g., Ref. [24]). This component is not driven by the derivatives of  $\bar{U}$ , but by the imposed shear flow  $\nabla_x \bar{U}_y^S$  itself. Indeed, one expects that this imposed shear leads to an  $xy$  stress

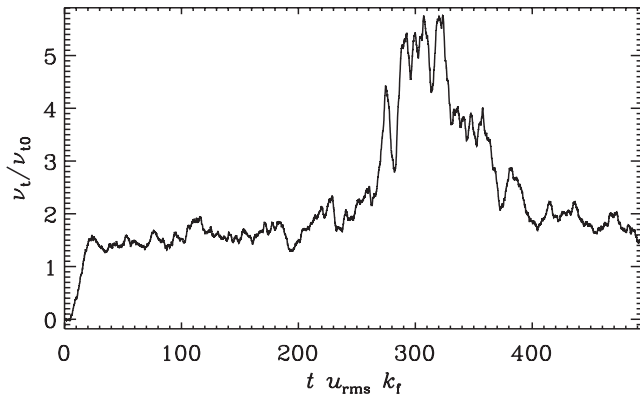


FIG. 11. Turbulent viscosity for run A, as obtained from the Reynolds stress component  $\bar{R}_{xy}$ , divided by the estimate  $\nu_{t0}$ .

$$\overline{u_x u_y} = -\nu_t (\nabla_x \bar{U}_y^S + \nabla_y \bar{U}_x^S) = -\nu_t S. \quad (21)$$

This is indeed the case; see Fig. 11. It turns out that the  $\nu_t$  determined in this way is rather similar to the value of  $\nu_{22}$  estimated from Eq. (20). Again, there is no good reason that these values are the same, because the eddy viscosity obtained from Eq. (21) belongs to a different component of the full rank-4 eddy viscosity tensor and is not part of the rank-2 tensor considered above.

## VI. CONCLUSIONS

The present work has demonstrated quite clearly that in nonhelical shear-flow turbulence a large-scale flow pattern emerges spontaneously. In the present case, where in the absence of shear the turbulence saturates at a Mach number of order 0.01, the large-scale flow becomes exceedingly strong and saturates at a Mach number of 0.1–0.2. This behavior is seen both at small and at the largest Reynolds numbers considered here (Re=100, based on the inverse forcing wave number).

The flow pattern can be particularly well pronounced at certain times and shows a long wavelength variation in the direction perpendicular to the plane of the shear flow (here the  $z$  direction). For negative shear, the  $x$  and  $y$  components of the shear flow are in phase in a way that is compatible with an interpretation in terms of a large-scale vorticity dynamo, as explored first by Elperin, Kleeorin, and Rogachevskii [14]. This means that the large-scale flow is driven by an anisotropic eddy viscosity tensor. Particularly important is its  $xy$  component  $\nu_{xy}$ , which describes the production of a cross-stream large-scale flow component  $\bar{U}_x(z, t)$  from a  $z$  variation of the streamwise large-scale flow  $\bar{U}_y(z, t)$ . The mean-vorticity “dynamo cycle” is completed by a suitable action of the shear itself, which produces a streamwise large-scale flow component  $\bar{U}_y$  from the cross-stream component  $\bar{U}_x$  by the term  $-\bar{U} \cdot \nabla \bar{U}^S$ .

The mean-vorticity dynamo cycle can only work if the sign of  $\nu_{xy}$  is the same as that of the shear  $\nabla_x \bar{U}_y^S$ . The present investigations suggest that this is indeed the case. However,

it is desirable to verify the sign of  $\nu_{xy}$  using a test-flow method analogously to the test-field method used in magnetohydrodynamics. Some care in using the correlation method is in order, because there are examples in magnetohydrodynamics where the correlation method give incorrect values for some components of the magnetic diffusion tensor, although other components were correct [25]. For example, when we apply a method analogous to that in Eq. (18) to the magnetic field of a simulation of shear flow turbulence (see, e.g., Figs. 7 or 8 of Ref. [12]), the components of the magnetic field scatter almost isotropically about the origin. This is compatible with an interpretation in terms of an incoherent  $\alpha$ -shear effect [12,26]. On the other hand, there is still a weak correlation with a negative slope. This would suggest that the shear-current dynamo might also be at work, even though the test-field method indicates that this should not be the case.

Clearly, the reality of the large-scale flow found in simulations is more complicated than what is suggested by the simple mean-vorticity dynamo problem. First, in contrast to the magnetic dynamo no kinematic stage can be distinguished, i.e., the large-scale patterns are visible only after they are already of dynamical importance. Secondly, the mean flow can reverse sign in random intervals which is not anticipated from the linear mean-vorticity dynamo model with anisotropic eddy viscosity, where self-excited solutions would always be nonoscillatory. Another question that needs to be addressed in future work is the saturation level of the large-scale flow, its relation to the saturation level of the small-scale flow, and a possible dependence on the Mach number.

For more realistic applications it will be important to get information about the full eddy viscosity, which is a rank-4 tensor [8]. In the present work, where the averages are only one dimensional, the eddy viscosity reduces to a rank-2 tensor. Finally, for astrophysical applications it should be pointed out that the gas in many shear flows is ionized and electrically conducting, giving rise to efficient dynamo action. The resulting mean Lorentz force from the small-scale magnetic field modifies the eddy viscosity in a way that suppresses the mean-vorticity dynamo. Details of this need to be investigated further. Another effect that can suppress the mean-vorticity dynamo is rotation [13]. This can be understood from the dispersion relation in that the addition of rotation leads, among other terms, to a  $-4\Omega^2$  term inside the squared brackets of Eq. (16) that always suppresses the mean-vorticity dynamo.

## ACKNOWLEDGMENTS

We thank an anonymous referee for offering suggestions regarding the break-down of the linearity of Eqs. (14) and (15). The computations were performed on the facilities hosted by the Center of Scientific Computing in Espoo, Finland, who are administered by the Finnish ministry of education. This work was supported by the Academy of Finland Grant No. 121431 (P.J.K.), the Leverhulme Trust (D.M.), and the Swedish Research Council (A.B.).

- [1] S. S. Moiseev, R. Z. Sagdeev, A. V. Tur, G. A. Khomenko, and V. V. Yanovskii, *Sov. Phys. JETP* **58**, 1149 (1983).
- [2] L. L. Kitchatinov, G. Rüdiger, and G. Khomenko, *Astron. Astrophys.* **287**, 320 (1994).
- [3] U. Frisch, Z. S. She, and P. L. Sulem, *Physica D* **28**, 382 (1987).
- [4] P. L. Sulem, Z. S. She, H. Scholl, and U. Frisch, *J. Fluid Mech.* **205**, 341 (1989).
- [5] B. Galanti and P.-L. Sulem, *Phys. Fluids A* **3**, 1778 (1991).
- [6] A. Brandenburg and B. von Rekowski, *Astron. Astrophys.* **379**, 1153 (2001).
- [7] G. Rüdiger, *Geophys. Astrophys. Fluid Dyn.* **16**, 239 (1980).
- [8] G. Rüdiger, *Differential Rotation and Stellar Convection: Sun and Solar-type Stars* (Gordon & Breach, New York, 1989).
- [9] I. Rogachevskii and N. Kleeorin, *Phys. Rev. E* **68**, 036301 (2003).
- [10] I. Rogachevskii and N. Kleeorin, *Phys. Rev. E* **70**, 046310 (2004).
- [11] T. A. Yousef, T. Heinemann, A. A. Schekochihin, N. Kleeorin, I. Rogachevskii, A. B. Iskakov, S. C. Cowley, and J. C. McWilliams, *Phys. Rev. Lett.* **100**, 184501 (2008).
- [12] A. Brandenburg, K.-H. Rädler, M. Rheinhardt, and P. J. Käpylä, *Astrophys. J.* **676**, 740 (2008).
- [13] T. A. Yousef, T. Heinemann, F. Rincon, A. A. Schekochihin, N. Kleeorin, I. Rogachevskii, S. C. Cowley, and J. C. McWilliams, *Astron. Nachr.* **329**, 737 (2008).
- [14] T. Elperin, N. Kleeorin, and I. Rogachevskii, *Phys. Rev. E* **68**, 016311 (2003).
- [15] G. Rüdiger and L. L. Kitchatinov, *Astron. Nachr.* **327**, 298 (2006).
- [16] T. A. Yousef, A. Brandenburg, and G. Rüdiger, *Astron. Astrophys.* **411**, 321 (2003).
- [17] A. Brandenburg, *Astrophys. J.* **550**, 824 (2001).
- [18] <http://www.nordita.org/software/pencil-code>
- [19] J. Wisdom and S. Tremaine, *Astron. J.* **95**, 925 (1988).
- [20] J. F. Hawley, C. F. Gammie, and S. A. Balbus, *Astrophys. J.* **440**, 742 (1995).
- [21] P. J. Käpylä and A. Brandenburg, e-print arXiv:0810.2298.
- [22] T. Elperin, I. Golubev, N. Kleeorin, and I. Rogachevskii, *Phys. Rev. E* **76**, 066310 (2007).
- [23] S. Sur, A. Brandenburg, and K. Subramanian, *Mon. Not. R. Astron. Soc.* **385**, L15 (2008).
- [24] P. J. Käpylä and A. Brandenburg, *Astron. Nachr.* **328**, 1006 (2007).
- [25] A. Brandenburg and D. Sokoloff, *Geophys. Astrophys. Fluid Dyn.* **96**, 319 (2002).
- [26] E. T. Vishniac and A. Brandenburg, *Astrophys. J.* **475**, 263 (1997).